Towards Isotropic Vortex Pinning in YBCO Films with Double-doping BHO-Y_2O_3 and BZO-Y_2O_3 Artificial Pining Centers

IOP Conf. Series: Materials Science and Engineering **279** (2017) 012030 doi:10.1088/1757-899X/279/1/012030

Towards Isotropic Vortex Pinning in YBCO Films with Double-doping BHO-Y_2O_3 and BZO-Y_2O_3 Artificial Pining Centers

Bibek Gautam[*1], Mary Ann Sebastian[2], Shihong Chen[1], Timothy Haugan[2], Yanbin Chen[3], Zhongwen Xing[4], Joseph Prestigiacomo[5], Mike Osofsky[5] and Judy Wu[*1]

[1]*Department of Physics and Astronomy, University of Kansas, Lawrence, Kansas 66045, USA*
[2]*U.S. Air Force Research Laboratory, Propulsion Directorate, WPAFB, OH 45433 USA*
[3]*Physics Department at Nanjing University, Nanjing, Jiangsu 210093, China*
[4]*College of Engineering and Applied Science, Nanjing University, Nanjing, Jiangsu 210093, China*
[5]*US Naval Research Laboratory, 4555 Overlook Ave, SW Washington, DC 20375, USA*

Email: gautbibe@ku.edu, jwu@ku.edu

Abstract. Strong and isotropic vortex pinning landscape is demanded for high field applications of $YaBa_2Cu_3O_{7-x}$ (YBCO) epitaxial thin films. Double-doping (DD) of artificial pinning centers (APCs) of mixed morphologies has been identified as a viable approach for this purpose. This work presents a comparative study on the transport critical current density $J_c(H, \theta)$ of 3.0 vol.%Y_2O_3+2.0 (or 6.0) vol.% $BaZrO_3$ (BZO DD) and 3.0 vol.%Y_2O_3+ 2.0 (or 6.0) vol.% $BaHfO_3$ (BHO DD) films. Based on the elastic strain model, $BaHfO_3$ (BHO) nanorods have lower rigidity than their $BaZrO_3$ (BZO) counterparts, which means their c-axis alignment is more susceptible to the local strain generated by the secondary dopant of Y_2O_3. Considering the increasing strain field with higher BZO (or BHO doping), the higher susceptibility may result in a large portion of the BHO APCs moving away from perfect c-axis alignment and enhancing isotropic pinning with respect to the H orientation. This is confirmed since the BHO DD films illustrate a less pronounced J_c peak at H//c-axis and hence more isotropic $J_c(\theta)$ than their BZO DD counterparts. At 9.0 T, the variation of the J_c across the entire θ range (0-90 degree) is less than 18% for the BHO DD film, in contrast to about 100% for the 2.0 vol.% BZO DD counterpart. At the higher BHO concentration of 6.0 vol.%, this higher tunability of the Y_2O_3 leads to increased ab-plane aligned BHO APCs and hence enhanced J_c at H//ab-plane.

1. Introduction

Artificial pinning centers (APCs) created by inserting impurity phase materials like $BaZrO_3$ (BZO), $BaSnO_3$ (BSO), $BaHfO_3$ (BHO), and $YBa_2(Nb/Ta)O_6$ in the film matrix have shown to provide an effective approach to enhance the critical current density J_c in applied magnetic fields (H) [1-7]. This has motivated efforts in controlling the APC morphology, dimension, orientation, and concentration for optimized $J_c(H, \theta, T)$. Double doping (DD) has been recently employed to generate APCs of mixed morphology such as 1D+3D APCs in BZO+Y_2O_3 [1, 8], BSO+Y_2O_3 [9, 10], BHO+Y_2O_3 [11], $BaTiO_3$+Y_2O_3 [12] and $Ba_2Y(Nb/Ta)O_6$ [13, 14] doped RE-123 matrices. The c-axis aligned 1D APCs can provide strong correlated pinning to address the weak pinning due to the layered structure of the RE-123. The 3D APCs have been found to further reduce the angular dependence of the J_c with respect to the H orientation. Among others, the BSO+Y_2O_3 (or Y211) doped YBCO thin films and conductors (BSO DD) have received most intensive study since BSO 1D APCs (or nanorods) have a relatively larger diameter of 7-10 nm [10] than the most other 1D APCs' and therefore remain their c-axis alignment in the BSO DD films in the moderate doping range [9, 11, 15]. 1D APCs of smaller diameters, such as BZO (5-6 nm) [3], BHO (4-5 nm) [2] are expected to have less rigidity and therefore are more susceptible to the local nonuniform strain field, induced by seeded growth, or DD, or vicinal growth, resulting in shorter segments of 1D APCs or splayed around the c-axis [7, 8, 16] An unique benefit of the more disordered APC landscape study is the reduced strain field overlap at high APC concentration

and hence reduced T_c degradation and improved J_c at 77 K. In DD format, 1D APCs of smaller diameters may allow high concentration doping for enhanced isotropic pinning.

Motivated by this, we investigate transport $J_c(H,\theta)$ in 2 and 6 vol.% BZO or BHO + 3 vol.% Y_2O_3 (BZO or BHO DD) in YBCO thin films. Although having comparable diameters of ~5-6 nm [17, 18], BZO 1D APCs have higher rigidity than their BHO counterparts according to an elastic strain model [19] with consideration of the lattice mismatch of APC and YBCO along with the elastic properties of both. The comparison of the 2 vol.% BZO and BHO DD films has revealed promising trend anticipated from the theory. At 9.0 T, for example, the variation of the J_c across the entire θ range (0-90 degree) is less than 18% for the BHO DD film, in contrast to about 100% for the 2 vol.% BZO DD counterpart. This work intends to further this study by including the 6 vol.% BZO and BHO DD films in this comparative study of the transport $J_c(H,\theta)$ at different temperatures (77 K and 65 K) and field up to 9.0 T at different orientation at $\theta = 0^o$ (H//c-axis), $\theta = 45^o$, and $\theta = 90^o$ (H//ab-plane). A strong and isotropic pinning can be achieved in the low concentration (2 vol. %) BHO DD film, a significant orientation switch of BHO APCs from c-axis aligned to ab-plane aligned occurs at 6 vol.% and hence improves J_c at $\theta=90^o$. This is in contrast to the well mixed APC morphology in 6 vol% BZO DD case.

2. Sample preparation and experiment

A fixed 3 vol.%Y_2O_3 and variable 2 and 6 vol.% $BaZrO_3$ or $BaHfO_3$ mixed with YBCO targets were used to fabricate two sets of BZO DD and BHO DD thin films on (100) $SrTiO_3$ (STO) single crystal substrates at their optimum growth temperatures 825 °C and 810 °C, respectively, using pulse laser deposition (PLD). PLD system utilizes a Lambda Physik LPX 300 KrF excimer laser of wavelength (λ) =248nm and a fluence of approximately 1.6 J/cm^2 for the depositions. All the films were deposited at laser energy of 450 mJ and a repetition rate of 8 Hz, within the 300 mTorr oxygen pressure which were annealed for 30 minutes at 500 ˚C within an oxygen environment after deposition. The thicknesses of the film were around 140 nm and 160 nm for BZO DD and BHO DD thin films, respectively.

For electrical transport measurement, two parallel microbridges of the width ~20 μm or ~40 μm and the length ~500 μm were patterned respectively using photolithography. Quantum Design Evercool II Physical Properties Measurement System (PPMS) with a vibrating sample magnetometer (VSM) was utilized for measuring the critical temperature (T_c) and the transport J_c (H) at H orientations of $\theta = 0^o$ (H//c-axis), 45°, and 90° (H//ab plane) in the plane where H is always perpendicular to J_c. Angular dependence $J_c(\theta)$ at different field was also measured for understanding isotropic pinning properties. To minimize sample heating effect short current pulses of width of 50 ms and pulse interval of 3.0 s were employed in the I-V measurement.

3. Results and discussions

Figures 1a-d compare the X-ray diffraction (XRD) θ-2θ spectra of 2 vol.% and 6 vol.% BZO DD or BHO DD films. The major diffraction (00l) peaks for all films indicate they are highly crystalline c-axis oriented. The c-axis lattice constants are 1.172 nm and 1.177 nm for 2 vol.% BZO and BHO DD respectively, and 1.173 nm for 6 vol. % BZO or BHO DD films. Some weak peaks are also observed which are attributed to either crystalline BZO (or BHO) or Y_2O_3 APCs. A distinctly larger full width at a half maximum (FWHM) of 2 vol. % BZO DD (0.839 deg.) compared to FWHM of 2 vol. % BHO DD (0.353 deg.) implies a more disturbance of lattice in former as compared to the latter. However, the comparable FWHM of 0.489 deg. and 0.567 deg., respectively for 6 vol. % BZO DD and BHO DD films suggests the difference in the YBCO lattice in the two cases reduces considerably at higher BZO (or BHO) concentrations.

Figures 2a-c compare the $J_c(H)$ curves in the field up to 9.0 T at H orientations of $\theta = 0^o$ (H//c-axis), θ=45°, and θ=90° (H//ab plane) for 2 vol.% BZO DD (circle) and BHO DD (inverted triangle) films measured at 65 K (open) and 77 K (solid and half filled). At 65 K, J_c(H//c-axis) is slightly higher for 2

vol.% BZO DD film at all field range up to 9.0 T while the lower $J_c(H)$ value of this sample at 77 K may be due to the lower T_c ~ 85.71 K for BZO DD film as compared to the T_c ~ 87.08 K for 2 vol.% BHO DD film. This same T_c effect may explain the lower $J_c(H)$ value of the 2 vol.% BZO DD film at θ=45°, and θ=90° (Figures 2b-c). Based on the comparison at 65 K, both 2 vol.% BZO DD and BHO DD samples have high-concentration c-axis aligned 1D APCs as indicated by the high $J_c(H)$ at H//c-axis. These 1D APCs act

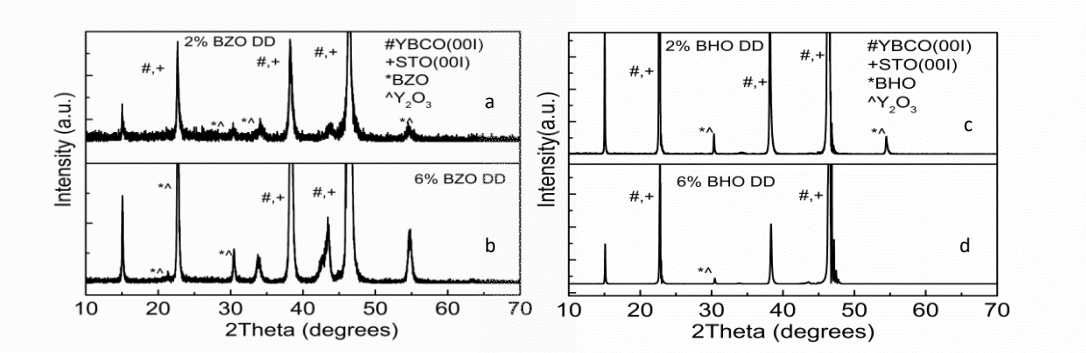

Figure 1. XRD θ-2θ scan for (a) 2 vol.%, (b) 6 vol.% BZO + 3 vol.% Y_2O_3 (BZO DD), and (c) 2 vol.%, (d) 6 vol.% BHO + 3 vol.% Y_2O_3 (BHO DD) doped YBCO thin films on STO substrates. Indices follow the same for the 2 and 6% BZO DD, and 2 and 6% BHO DD respectively.

as strong correlated pinning centers up to the so called matching field H=n*ϕ_0, where n is the areal density of 1D APCs in c-axis and ϕ_0 is the flux quantum. Quantitatively, this enhanced pinning can be described by the α value through fitting of $J_c(H)$~$H^{-\alpha}$. For reference, YBCO films without APCs, α~0.5-0.6 [20]. The enhanced pinning in the 2 vol.% DD samples is illustrated in the much reduced α value ~ 0.17 and 0.16 for the 2 vol.% BZO DD and BHO DD respectively. At 65 K, the trend at θ=45°, indicates the enhanced pining at wide angular range is probably due to misaligned 1D APCs rather by splayed BHO 1D APCs which probably could pin the vortices in small angular range (Figure 2b). Interestingly, at 65 K, J_c (H // ab-plane) overcomes for 2 vol. % BHO DD film at higher field (>2.0 T) which can be seen as the crossover of the J_c at round 2.0 T (Figure 2c). This crossover trend of J_c(H) value at θ=45° and θ=90° is an indication of strong pinning ability of BHO APCs not only along ab-plane but also the angle between c-axis and ab-plane. Such enhancement at wide angular range may possibly due to the formation of misaligned and short BHO APCs in the film by influence of kinematic diffusion of BHO along c-axis in the presence of Y_2O_3.

In parallel, the $J_c(H)$ curves of the 6 vol.% BZO DD (circle) and BHO DD (inverted triangle) measured at the same conditions are compared in Figures 2d-f. With the increasing BZO and BHO doping to 6 vol.%, the overall $J_c(H$//c-axis) is higher for BZO DD film for the entire field range 0-9.0 T, and at both temperature 77 K and 65 K. Interestingly, the T_c values for 6 vol.% BHO DD film reduces to 85.8 K in contrast to T_c ~ 87.8 K for 6 vol.% BZO DD films. Despite of similar PLD sample fabrication process was used to these films, 3 vol.% Y_2O_3 influenced differently in pinning landscape. The increase T_c for 6 vol.% BZO DD film is probably through reducing strain field overlap, is also observed in 6 vol.% BZO single doped YBCO film on vicinal substrate [3]. Since $J_c(H)$~effective length of APCs, the higher $J_c(H$//c-axis) at 65 K for 6 vol.% BZO DD possibly due to longer effective c-axis aligned 1D APCs. The similar trend with comparable $J_c(H$ at θ=45°) for both 6 vol.% BZO and BHO DD films observed at 65 K, where T_c effect is negligible, implies comparable pinning strength of 1D APCs (Figure 2e). Interestingly, at 65 K, J_c (H // ab-plane) overcomes for 6 vol.% BHO DD film at higher field (>2.0 T) same as the 2 vol.% BHO DD film. The slow decrease of J_c at high field when H // ab-plane or about 1.7 times higher $J_c(H$ // ab-plane) in average for the entire field upto 9.0 T compared to $J_c(H$ // c-axis) at 65 K for 6 vol.% BHO DD indicates the strong pinning possibly due to ab-aligned BHO 1D APCs.

However, the reverse results are observed in 6 vol.% BZO DD film in which higher $J_c(H)$ along c-axis compared to ab-plane. The higher J_c (H // ab-plane) may be due to strong intrinsic pinning of layered structure or intrinsic pining plus 1D APCs aligned along ab-plane. The former may cause sharp $J_c(\theta)$ at $\theta=90^o$ while latter may cause wider peak at around $\theta=90^o$. The latter may be more convincing in this case as we have observed wider $J_c(\theta=90^o)$ [details in later section].

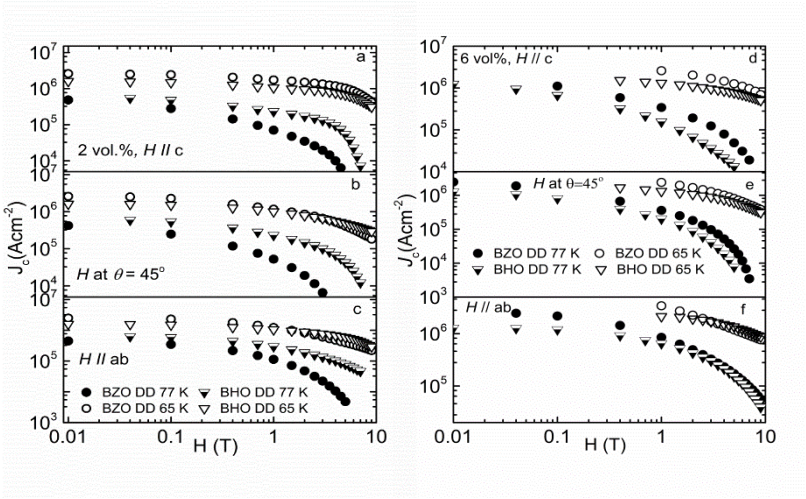

Figure 2. J_c vs. H curves measured on 3% Y_2O_3+2% BZO or BHO doped YBCO (BZO (circle) or BHO (inverted triangle) DD) nanocomposite films at (a) $\theta=0^o$ (H//c-axis), (b) $\theta=45^o$, and (c) $\theta=90^o$ (H//ab-plane) and 3% Y_2O_3+6% BZO or BHO doped YBCO (BZO or BHO DD) nanocomposite films at (d) $\theta=0^o$ (H//c-axis), (e) $\theta=45^o$, and (f) $\theta=90^o$ (H//ab-plane) at 77 K (solid and half filled) and 65 K (open) respectively.

Figures 3a-c compare the field dependence of the pining force density $F_p=J$ x H at 77 K and 65 K at field ordination $\theta=0^o$ (H // c-axis), $\theta=45^o$ and $\theta=90^o$ (H // ab-plane) for 2 vol.% BZO or BHO DD film. Except H at $\theta=90^o$ for 2 vol.% BZO DD film, F_p vs H curve show the typical inverted bell shape with different F_p peak location (H_{max}) and peak value $F_{p,max}$. At H // c-axis (Figure 3a), the H_{max}, representing so called matching field, are comparable for BZO and BHO APCs at 65 K, explore the comparable number density of APCs are effectively acting along c-axis. Noticeably high $F_{p,max}$ (~ 1.5 times) for BZO DD compared to BHO DD films at 65 K, where T_c effect is negligibly small, support the argument of strong F_p (=n*f_p , n is the effective no density of APCs and f_p is the pinning force per unit length of APCs) through longer BZO 1D APCs aligned to c-axis. Interestingly, the same trend is not followed when H at $\theta=45^o$ and H // ab-plane (Figures 3b and 3c) at 65 K. At both temperatures, the $F_{p,max}$ and H_{max} are higher for BHO DD films especially the cross-over of $F_{p,max}$ at 4.5 T and 2.5 T respectively, is an indication of increasing effectiveness of the BHO 1D APCs. In addition, at 65 K, and H at $\theta=45^o$, $F_{p,max}$~ 26.71 GN/m^3, and H_{max}~8.5 T are about 1.14 and 2.0 times higher respectively for BHO DD film compared to its counterpart. The similar trend of $F_{p,max}$ and H_{max} are observed at H // ab-plane (Figure 3c). It further implies that the addition of 3 vol.% Y_2O_3 influence more on orientation and morphology of BHO APCs compared to BZO APCs due to higher tunability of BHO as predicted theoretically in our other paper [21].

In addition, Figures 3d-f compare the F_p vs H curves measured at the same condition for 6 vol.% BZO or BHO DD film respectively. The higher $F_{p,max}$ are observed for BZO DD films except when H // ab-plane, at which $F_{p,max}$ overtakes for BHO DD film. At 65 K, when H // c-axis, $F_{p,max}$ ~ 67.99 GN/m^3 for BZO DD is about 1.5 times in contrast to BHO DD $F_{p,max}$~ 45.78 GN/m^3 but lower H_{max}~7.0 T for former compared to H_{max}~8.5 T latter. It means weaker pinning strength (measured through H_{max}) of

BZO APCs compared to BHO APCs along c-axis. Interestingly, $F_{p,max}$ gap decreases when H at θ=45° (Figure 3e) with $F_{p,max}$~40.65 GN/m^3 for BZO DD. It is only about 1.3 times higher than BHO DD.

But the higher H_{max}~6.0 T for BHO DD compared to 4.5 T for its counterpart. It is indicative of higher pinning strength possibly due to high effective areal density of misaligned BHO APCs. At 65 K, the constant difference of H_{max} (1.5 T) when H // c-axis and H at θ=45° for both films suggest the equable pining strength of BZO and BHO APCs along those directions. However, the same trend is not followed for the field (H) // ab-plane (Figure 3f). The higher $F_{p,max}$ >78.63 GN/m^{3}for BHO DD is an indicative of the strong pinning by BHO APCs in contrast to BZO APCs ($F_{p,max}$ ~68.72 GN/m^3). More interestingly, the constant gap of $F_{p,max}$ beyond 6.0 T, at H // ab-plane explores the fact that the almost an equal number of effective 1D APCs are involved in vortex pinning in both cases. The bell shaped F_p vs H curve for 2 vol.% BHO DD film has changed to constantly increasing $F_{p,max}$ at H>6.0 T for 6 vol.% BHO DD also suggests that BHO APCs has more tunability in the presence of Y_2O_3 in contrast to BZO APCs. It further suggests that the orientation of 1D APCs more likely changes from c-axis alignment to ab-plane alignment with increasing BHO concentration to 6 vol.% compared to similarly doped BZO film (Figures 3c and 3f). This result is different from BZO DD case in which 6 vol.% BZO DD film shows more isotropic at low temperature (≤ 65 K) in compared to lower BZO concentration [1]. This indicates that the BZO APCs in DD film may provide effective APCs along with Y_2O_3 improving vortex pinning for the field orientation other than c-axis.

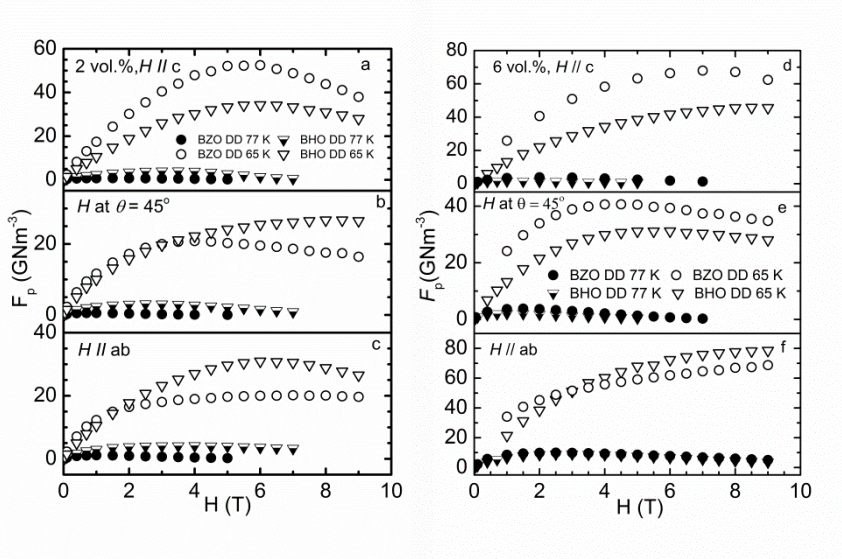

Figure 3. F_p vs. H curves measured on 3% Y_2O_3+2% BZO or BHO doped YBCO (BZO (circle) or BHO (inverted triangle) DD) nanocomposite films at (a) θ=0° (H//c-axis), (b) θ= 45°; and (c) ,θ= 90° (H//ab-plane) and 3% Y_2O_3+6% BZO or BHO doped YBCO (BZO or BHO DD) nanocomposite films at (d) θ=0° (H//c-axis), (e) θ= 45°; and (f) ,θ= 90° (H//ab-plane) at 77 K (solid and half filled) and 65 K (open) respectively.

Based on the discussion so far, the schematic of the BZO, BHO and Y_2O_3 nanostructures morphology and orientation in BZO DD (a,c) and BHO DD (b,d) films can be schematically represented as in Figures 4a-d. At low concentration (2 vol.%), the orientation of 1D-APCs may be perpendicular to the surface (c-axis of the film), but they may form more splayed and short APCs in BHO DD compared to BZO DD film. However, at higher concentration (6 vol.%), 1D APCs may noticeably be either parallel or perpendicular to the surface (ab-plane or c-axis) of the films. Due to the higher rigidity of BZO compared to BHO, the majority of the BZO 1D APCs may form along c-axis of the film in contrast to BHO 1D APCs along ab-plane (Figures 4c and 4d).

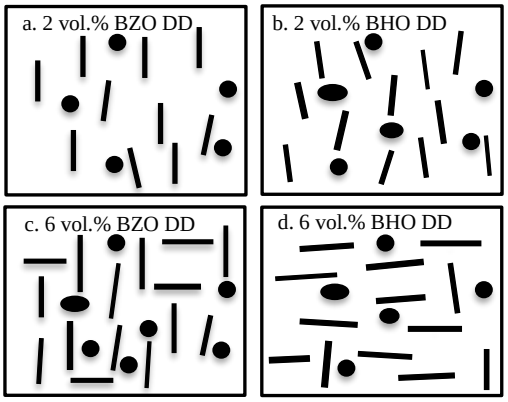

Figure 4. Schematic of the distribution of the 1D APCs (rod shape) and 3D APCs (spherical or oval shape) nanostructures in the YBCO films with (a) 2 vol.% and (c) 6 vol.% BZO DD films, (b) 2 vol.% and (d) 6 vol.% BHO DD films.

Figures 5a-b compare the $J_c(\theta)$ curves at 65 K, for 2 vol.% and 6 vol.% BZO and BHO DD films respectively. The differences in $J_c(\theta)$ curves of 2 vol.% BZO and BHO DD films (Figure 5a) are the lower $J_{c,max}$ (J_c peak value) and higher $J_{c,min}$ (the lowest J_c value of the $J_c(\theta)$ curve) for the entire angular range $\theta=0^o$-90^o in BHO DD film compared to BZO DD film at 5.0 and 9.0 T. The reducing value of $J_{c,min}$ indicates weaker vortex pinning in that angular range while increasing $J_{c,max}$ is indicative of strong pinning by parallel 1D APCs aligned either along the c-axis or ab-plane. The J_c anisotropy (($J_{c,max}$ - $J_{c,min}$)/$J_{c,min}$) is about 129% for the BZO DD film at 5.0 T in contrast to 47% for its counterpart BHO DD (Figure 5a). J_c anisotropy further reduces to 100% at 65 K and 9.0 T for BZO DD film which is still 5 times higher than the J_c anisotropy of BHO DD film at same field and temperature. This indicates that at lower concentration (2 vol.%) BHO DD film shows more isotropic pinning compared to its counterpart BZO DD film.

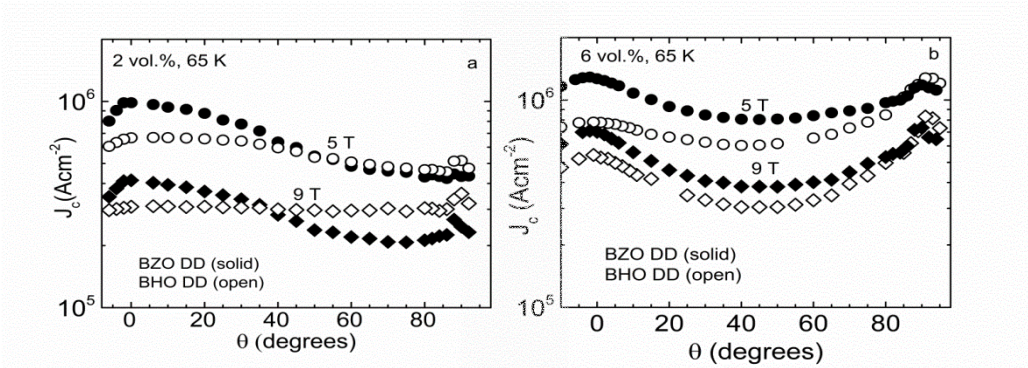

Figure 5. Angular dependence of J_c measured on (a) 3% Y_2O_3+2 vol% BZO or BHO doped YBCO (BZO(solid) or BHO (open) DD) (b) 3% Y_2O_3+6 vol% BZO or BHO doped YBCO (BZO or BHO DD) nanocomposite films measured at 5.0 T (circle), and 9.0 T (diamond) at 65 K.

However, this trend doesn't follow for the 6 vol. % DD films. At 65 K, the overall J_c is higher for 6 vol% BZO DD film for the entire angular range as defined previously at 5.0 T and 9.0 T. Thus, an increase of $J_c(\theta)$ value for wide angular range for BZO DD film is indicative of strong and effective pinning by 1D APCs along with 3D APCs for the field other than c-axis compared to BHO DD film. Comparing 2 vol.% DD films, J_c peaks are observed at H // c-axis and H // ab-plane for both 6 vol.% DD films. There is an absence of such peak at H // c-axis in 2 vol.% BHO DD film appears at 6 vol.% BHO DD films. The J_c anisotropy of 6 vol.% BZO DD at 5.0 T is about 60% compared to 111% for BHO DD film. In addition, at 9.0 T, J_c anisotropy is about 92% for the BZO DD film which is almost half of the BHO DD film (173%). The increasing J_c anisotropy in BHO DD film may be due to

increasing J_c peak towards the ab-plane rather than J_c peak at c-axis which is different from BZO DD film at which J_c peaks appear at around c-axis. It means at 6 vol.% BZO DD film, more isotropic pinning is observed in contrast to BHO DD film. This illustrates that the influence of Y_2O_3 in BZO and BHO 1D-APCs is different, more in the latter compared to former.

4. Conclusion

A comparative study of the transport J_c (H, θ) of the BZO DD and BHO DD films has been carried out at 77 K and 65 K, in magnetic field up to 9.0 T. A secondary Y_2O_3 3D APC doping was employed to probe the susceptibility of the c-axis alignment of BZO and BHO nanorods to the local strain generated by the Y_2O_3 3D APC. At a fixed 3.0 vol.% of Y_2O_3 3D APC doping, the concentration of the BZO and BHO nanorods was varied from 2.0 vol.% to 6.0 vol.%. At the 2.0 vol.% concentration, the BHO DD film shows more isotropic pinning in the entire field range at 65 K, reducing J_c anisotropy. At the higher concentration of 6.0 vol.%, the overall higher J_c(θ) values are observed in BZO DD samples for wide angular range from H//c-axis at 65 K except around H//ab-plane. This may be attributed to the switch of a larger proportion of the BHO APCs to ab-plane alignment at the higher strain field overlap as compared to the BZO counterparts. Consequently, the J_c anisotropy increased from 18 % at 2.0 vol.% to 173% at 6.0 vol.% BHO concentration in BHO DD films at 9.0T and 65 K. This is in contrast to the opposite trend of the J_c anisotropy of 100% to 92% at the same condition in BZO DD films as the BZO concentration was increased from 2.0 vol.% to 6.0 vol %. This result illustrates the importance of understanding the effect of the strain field on the APC morphology via DD and other approaches.

5. References

[1] S. Chen, M. Sebastian, B. Gautam, J. Wilt, T. Haugan, Z. Xing*, et al.*, "Enhancement of Isotropic Pinning Force in YBCO Films With $BaZrO_3$ Nanorods and Y_2O_3 Nanoparticles," *IEEE Transactions on Applied Superconductivity,* vol. 27, pp. 1-5, 2017.

[2] S. Miura, Y. Yoshida, Y. Ichino, Q. Xu, K. Matsumoto, A. Ichinose*, et al.*, "Improvement in J c performance below liquid nitrogen temperature for SmBa2Cu3O y superconducting films with BaHfO3 nano-rods controlled by low-temperature growth," *APL Materials,* vol. 4, p. 016102, 2016.

[3] J. Wu, J. Shi, F. Baca, R. Emergo, J. Wilt, and T. Haugan, "Controlling $BaZrO_3$ nanostructure orientation in $YBa_2Cu_3O_7$ films for a three-dimensional pinning landscape," *Superconductor Science and Technology,* vol. 28, p. 125009, 2015.

[4] M. Erbe, J. Hänisch, R. Hühne, T. Freudenberg, A. Kirchner, L. Molina-Luna*, et al.*, "BaHfO3 artificial pinning centres in TFA-MOD-derived YBCO and GdBCO thin films," *Superconductor Science and Technology,* vol. 28, p. 114002, 2015.

[5] M. A. P. Sebastian, J. N. Reichart, J. L. Burke, and L. B. Brunke, "Optimizing Flux Pinning of YBCO Superconductor with $BaSnO_3$+ Y2O3 Dual Mixed Phase Additions," *Optimizing Flux Pinning of YBCO Superconductor with $BaSnO_3$+ Y2O3 Dual Mixed Phase Additions,* 2013.

[6] X. Obradors, T. Puig, S. Ricart, M. Coll, J. Gazquez, A. Palau*, et al.*, "Growth, nanostructure and vortex pinning in superconducting YBa2Cu3O7 thin films based on trifluoroacetate solutions," *Superconductor Science and Technology,* vol. 25, p. 123001, 2012.

[7] F. Baca, P. Barnes, R. Emergo, T. Haugan, J. Reichart, and J. Wu, "Control of $BaZrO_3$ nanorod alignment in $YBa_2Cu_3O_{7-x}$ thin films by microstructural modulation," *Applied Physics Letters,* vol. 94, p. 102512, 2009.

[8] B. Maiorov, S. A. Baily, H. Zhou, O. Ugurlu, J. A. Kennison, P. C. Dowden*, et al.*, "Synergetic combination of different types of defect to optimize pinning landscape using $BaZrO_3$ doped $YBa_2Cu_3O_7$," *Nature materials,* vol. 8, pp. 398-404, 2009.

[9] A. K. Jha, K. Matsumoto, T. Horide, S. Saini, P. Mele, Y. Yoshida*, et al.*, "Systematic Variation of Hybrid APCs Into YBCO Thin Films for Improving the Vortex Pinning Properties," *IEEE Transactions on Applied Superconductivity,* vol. 25, pp. 1-5, 2015.

[10] P. Mele, K. Matsumoto, A. Ichinose, M. Mukaida, Y. Yoshida, S. Horii*, et al.*, "Systematic study of $BaSnO_3$ doped $YBa_2Cu_3O_{7-x}$ films," *Physica C: Superconductivity,* vol. 469, pp. 1380-1383, 2009.

[11] M. A. P. Sebastian, J. N. Reichart, M. M. Ratcliff, T. J. Bullard, J. L. Burke, C. R. Ebbing*, et al.*, "Study of the Flux Pinning Landscape of YBCO Thin Films With Single and Mixed Phase Additions BaMO3+ Z: M= Hf, Sn, Zr and Z= Y2O3, Y211," *IEEE Transactions on Applied Superconductivity,* vol. 27, pp. 1-5, 2017.

[12] W. Hong-Yan, D. Fa-Zhu, G. Hong-Wei, and Z. Teng, "Strongly enhanced flux pinning in the YBa2Cu3O7− x films with the co-doping of BaTiO3 nanorod and Y2O3 nanoparticles at 65 K," *Chinese Physics B,* vol. 24, p. 097401, 2015.

[13] M. Sieger, P. Pahlke, M. Lao, M. Eisterer, A. Meledin, G. Van Tendeloo*, et al.*, "Tailoring Microstructure and Superconducting Properties in Thick BaHfO3 and Ba2 Y (Nb/Ta) O6 Doped YBCO Films on Technical Templates," *IEEE Transactions on Applied Superconductivity,* vol. 27, pp. 1-7, 2017.

[14] F. Rizzo, A. Augieri, A. Angrisani Armenio, V. Galluzzi, A. Mancini, V. Pinto*, et al.*, "Enhanced 77 K vortex-pinning in Y Ba2Cu3O7− x films with Ba2Y TaO6 and mixed Ba2Y TaO6+ Ba2Y NbO6 nano-columnar inclusions with irreversibility field to 11 T," *APL Materials,* vol. 4, p. 061101, 2016.

[15] T. Horide, T. Kawamura, K. Matsumoto, A. Ichinose, M. Yoshizumi, T. Izumi*, et al.*, "Jc improvement by double artificial pinning centers of $BaSnO_3$ nanorods and Y_2O_3 nanoparticles in $YBa_2Cu_3O_7$ coated conductors," *Superconductor Science and Technology,* vol. 26, p. 075019, 2013.

[16] R. L. S. Emergo, F. J. Baca, J. Z. Wu, T. J. Haugan, and P. N. Barnes, "The effect of thickness and substrate tilt on the BZO splay and superconducting properties of $YBa_2Cu_3O_{7-x}$ films," *Superconductor Science and Technology,* vol. 23, p. 115010, 2010.

[17] H. Tobita, K. Notoh, K. Higashikawa, M. Inoue, T. Kiss, T. Kato*, et al.*, "Fabrication of $BaHfO_3$ doped $Gd1Ba_2Cu_3O_{7-\delta}$ coated conductors with the high Ic of 85A/cm-w under 3T at liquid nitrogen temperature (77 K)," *Superconductor Science and Technology,* vol. 25, p. 062002, 2012.

[18] J. F. Baca, T. J. Haugan, P. N. Barnes, T. G. Holesinger, B. Maiorov, R. Lu*, et al.*, "Interactive Growth Effects of Rare‐Earth Nanoparticles on Nanorod Formation in $YBa_2Cu_3O_x$ Thin Films," *Advanced Functional Materials,* vol. 23, 2013.

[19] J. J. Shi and J. Z. Wu, "Micromechanical model for self-organized secondary phase oxide nanorod arrays in epitaxial $YBa_2Cu_3O_{7-\delta}$ films," *Philosophical Magazine,* vol. 92, pp. 2911-2922, 2012.

[20] V. Matsui, V. Flis, V. Moskaliuk, A. Kasatkin, N. Skoryk, and V. Svechnikov, "Current-carrying abilities of nano-structured HTS thin films," *J. Nanoscience Nanoengineering,* vol. 1, pp. 38-43, 2015.

[21] B. Gautam, M. A. Sebastian, S. Chen, J. Shi, T. Haugan, Z. Xing*, et al.*, "Transformational dynamics of BZO and BHO nanorods imposed by Y2O3 nanoparticles for improved isotropic pinning in YBa2Cu3 O 7-δ thin films," *AIP Advances,* vol. 7, p. 075308, 2017.

Acknowledgements

This research was supported in part by NSF contracts Nos. NSF-DMR-1337737 and NSF-DMR-1508494, the AFRL Aerospace Systems Directorate, and the Air Force Office of Scientific Research (AFOSR), the US National Science Foundation (DMR-1565822) for TEM characterization